Multiscale Partial Symbolic Transfer Entropy for Time-Delay Root Cause Diagnosis in Nonstationary Industrial Processes

Shuyu Duan, Chunhui Zhao, *Senior Member, IEEE*, and Min Wu, *Fellow, IEEE*

***Abstract*—Nonstationary characteristics and lack of time delays analysis remain two large obstacles to diagnosing fault root cause in industrial processes. However, ignoring these two issues, many traditional methods tend to introduce some spurious or indirect causal relationships that interfere with root cause judgments. In this article, multiscale partial symbolic transfer entropy (MPSTE) is proposed to handle the above-mentioned problems. On the one hand, a multivariate multiscale filter module of MPSTE is designed to estimate the information transfer on multiple time scales and detect time delays while considering the indirect causality of the multivariate industrial system. On the other hand, to capture the causal information from the nonstationary processes, MPSTE introduces a segmental symbolization procedure and maps time series into finite rank vectors, overcoming the limitation of stationarity. Moreover, two causal criteria for MPSTE are constructed to identify the direction and significance level of causality correspondingly. MPSTE can thus provide sufficient information for causal relationships and exclude spurious causality. Finally, a causal diagram construction strategy with time delay based on MPSTE is established to diagnose the root cause and trace the fault propagation path. The results of experimental verification in a coal mill rig prove the effectiveness of the proposed strategy.**

***Index Terms*—Causal inference, nonstationary industrial processes, root cause diagnosis, symbolic transfer entropy (STE), time delay estimation.**

Manuscript received 4 November 2021; revised 12 November 2021 and 8 February 2022; accepted 11 March 2022. Date of publication 29 March 2022; date of current version 5 October 2022. This work was supported in part by the National Science Fund for Distinguished Young Scholars under Grant 62125306, in part by the National Natural Science Foundation of China under Grant 62133003, and in part by the Research Project of the State Key Laboratory of Industrial Control Technology, Zhejiang University, China under Grant ICT2021A15. *(Corresponding author: Chunhui Zhao.)*

Shuyu Duan and Chunhui Zhao are with the College of Control Science and Engineering, Zhejiang University, Hangzhou 310027, China (e-mail: shuyuduan@zju.edu.cn; chhzhao@zju.edu.cn).

Min Wu is with the School of Automation, China University of Geosciences, Wuhan 430074, China, with the Hubei Key Laboratory of Advanced Control and Intelligent Automation for Complex Systems, Wuhan 430074, China, and also with the Engineering Research Center of Intelligent Technology for Geo-Exploration, Ministry of Education, Wuhan 430074, China (e-mail: wumin@cug.edu.cn).

Color versions of one or more figures in this article are available at https://doi.org/10.1109/TIE.2022.3161761.

Digital Object Identifier 10.1109/TIE.2022.3161761

I. Introduction

COMPLEX industrial processes are controlled by millions of coupled control loops with various physical and chemical reactions occurring throughout the process [1]. When faults happen, the abnormality spreads and influences plenty of the process variables, causing flood of alarms and overwhelming the operators. In practice, process monitoring [2], [3] and fault diagnosis [4], [5] have been widely used to prevent incipient faults in the industrial field, including high-speed trains [6] and autonomous vehicles [7]. In addition, if faults have spread for a while, root cause diagnosis task become more important, which can improve the efficiency of troubleshooting and avoid economic losses.

Root cause diagnosis aims to locate the root of fault by analyzing the causality between fault variables and clarifying the fault propagation path. For the above goal, the key is an appropriate causal inference method. In recent years, many data-driven causal analysis methods, such as Granger causality (GC) [8], transfer entropy (TE) [9], and convergent cross-mapping (CCM) [10], have been applied to diagnose the root cause. Most methods mentioned above were developed for stationary time series. However, real industrial processes generally show nonstationary characteristics, reflected by the time-variant mean or autocovariance [11]. The nonstationarity of processes is generally caused by various factors, such as operation condition changes, frequent product changes, unmeasured interference, and facility aging [12], [13]. In such case, the traditional methods show various shortages. On the one hand, the causal inference method based on a regression model like GC may be induced by similar trends of nonstationary processes, inferring spurious causality [14]. On the other hand, nonstationary variables usually cannot fulfill the prerequisite assumption of Gaussian distribution, which invalidates TE and its variants [15].

To overcome the limitations, researchers studied how to infer causality from nonstationary time series. Cointegration [12], [16] and symbolization [17] are representatives of such methods, which are initially developed for financial applications. VECM [16] introduces cointegrated variables to balance the short-term dynamics and the long-term tendencies. However, the study of VECM is restricted to nonstationary variables that are integrated of the same order [12], which is too strict for most processes. To solve this problem, researchers proposed symbolic transfer entropy (STE) [17] and partial symbolic transfer entropy (PSTE)

[18] based on rank vectors. By segmenting and ranking the nonstationary time series, STE and PSTE translate original data into stationary symbolic ones, adapting various nonstationary data in finance market. Although STE is helpful in dealing nonstationary series, it cannot analyze time delays between variables. While in practice, the critical issue is how to estimate time delays of causality and clarify the information transfer mechanisms from nonstationary processes.

In real industrial processes, time delays reflect how process variables influence each other through feedback control loops under dynamic noise [19]. Without time delays information, many indirect causalities cannot be eliminated [20]. More seriously, ignoring time delays means that the speed of fault propagation is unknown which may lead to severe accidents [21]. Thus, some research works have been proposed to improve traditional methods for time delay detection [22]. Ye [23] developed extended CCM (ECCM) to estimate time delays through the comparison of the cross-map lags. But the performance of ECCM is unstable, affected by too many parameters. To overcome this limitation, some studies like multiscale TE [24] and multiscale symbolic phase transfer entropy (MSPTE) [25] integrate multiscale analysis and TE to identify dynamic information flow between two variables on multiple scales. These methods inspire us to detect the time delay of causality. However, there remain some problems for practical industrial applications, including indirect influence from other variables and the adaptability of nonstationary situations.

In this work, the crucial issues are how to develop an elegant model that can infer nonstationary causality and detect the corresponding time delays simultaneously and how to apply it for root cause diagnosis of practical industrial processes. A multiscale partial symbolic transfer entropy (MPSTE) is proposed to handle the problems mentioned above. First, MPSTE takes a multivariate multiscale filler module to analyze information transfer in multiple time scales. Thus, time delays can be detected through the changing trend of MPSTE on multiple scales. For MPSTE, the nonstationary characteristic can be adapted with partial symbols, segmenting time series into rank vectors and capturing dynamic information. Second, two causal criteria for MPSTE are designed to calculate the direction and the significant level of causality and avoid ambiguity caused by bidirectional causality. One is a direct indicator based on the physical meaning of MPSTE, the other is a significant test that employs resampling techniques to obtain its empirical null distribution. Third, for real-world application, a strategy is established to construct a causal diagram with time delay from nonstationary fault data. The influence of indirect causality from multiple variates and different time delays is also considered to simplify the causal diagram. Finally, the root cause can be highlighted for the operators and the fault propagation path is revealed from the causal diagram.

The main contributions of this article are summarized as follows:

1) For the first time, the MPSTE model that simultaneously achieves nonstationary adaption and time delay detection is proposed to infer causality for multivariate nonstationary industrial processes. Furthermore, it also considers the indirect effect from other variables, improving its performance in industrial applications.
2) Two complementary causal criteria of MPSTE are designed for determining causal direction between nonstationary variables, avoiding confusing bidirectional causality.
3) A novel strategy to construct a causal diagram with time delay is developed for root cause diagnosis in nonstationary processes, tracing the fault propagation path and delay with a concise directed diagram. Time delays of causality can clarify the initial causal diagram and highlight the root cause variable.

II. Preliminaries

STE [17] and its multivariate version PSTE [18] are proposed for estimating information transferred among nonstationary time series. They have been widely used in finance [18]. Considering a multivariate system, the number of observed variables in the system is denoted as M. X and Y are two probing variables, Z represents the set of remaining variables. The delay vectors for X and Y are defined as $\mathbf{x_t} = [x_t, x_{t-t'_1}, \ldots, x_{t-(k-1)t'_1}]$ and $\mathbf{y_t} = [y_t, y_{t-t'_2}, \ldots, y_{t-(l-1)t'_2}]$. k and l are the corresponding embedding dimensions of X and Y. t'_1 and t'_2 are the sample intervals in embedding vectors.

Consider the delay vectors of variable X at an arbitrary time point t denoted by $\mathbf{x_t} = [x_t, x_{t-t'}, \ldots, x_{t-(k-1)t'}]$, arranging the k amplitude values in ascending order. Thus, the newly ordered series can be written as $x_{t-(r_{t,1}-1)t'} \leq x_{t-(r_{t,2}-1)t'} \leq \ldots \leq x_{t-(r_{t,m}-1)t'}$ where $r_{t,j}(j = 1, 2, \ldots, k) \in \{1, \ldots, k\}$ is the unique sequential symbol of the corresponding amplitude value. By this means, every delay vector is mapped into a unique rank vector which is one of $k!$ possible permutations, where $k! = k \times (k-1) \times \ldots \times 1$ denotes the factorial of k. The rank vector of X is defined as $\tilde{\mathbf{x}}_\mathbf{t} = (r_{t,1}, r_{t,2}, \ldots, r_{t,k})$.

For X and Y, each $\mathbf{y_t}$ and $\mathbf{x_t}$ are translated into rank vectors as $\tilde{\mathbf{y}}_\mathbf{t}$ and $\tilde{\mathbf{x}}_\mathbf{t}$. In this way, X and Y can be translated into symbol sequences $\tilde{X}$ and $\tilde{Y}$. The same goes for the remained variables of Z and $\tilde{\mathbf{z}}_\mathbf{t}$ is the rank vector of set Z (It is concatenated by the rank vectors of each of the variables in Z). Then PSTE can be written as

$$T^{\text{sym}}_{X\to Y|Z} = \sum_{y\in\mathcal{Y}, x\in\mathcal{X}, \mathbf{z}\in\mathcal{Z}} p(\tilde{\mathbf{y}}_{\mathbf{t+h}}, \tilde{\mathbf{y}}_\mathbf{t}, \tilde{\mathbf{x}}_\mathbf{t}, \tilde{\mathbf{z}}_\mathbf{t}) \times \log \frac{p(\tilde{\mathbf{y}}_{\mathbf{t+h}} | \tilde{\mathbf{y}}_\mathbf{t}, \tilde{\mathbf{x}}_\mathbf{t}, \tilde{\mathbf{z}}_\mathbf{t})}{p(\tilde{\mathbf{y}}_{\mathbf{t+h}} | \tilde{\mathbf{y}}_\mathbf{t}, \tilde{\mathbf{z}}_\mathbf{t})} \tag{1}$$

where $T^{\text{sym}}_{X\to Y|Z}$ is the value of PSTE. The joint and conditional probability $p(\tilde{\mathbf{y}}_{\mathbf{t+h}}, \tilde{\mathbf{y}}_\mathbf{t}, \tilde{\mathbf{x}}_\mathbf{t}, \tilde{\mathbf{z}}_\mathbf{t})$ and $p(\tilde{\mathbf{y}}_{\mathbf{t+h}} | \tilde{\mathbf{y}}_\mathbf{t}, \tilde{\mathbf{x}}_\mathbf{t}, \tilde{\mathbf{z}}_\mathbf{t})$ are calculated as relative frequency of the sequence of permutation indices. h is the prediction range.

Using rank vectors, PSTE translates the nonstationary data into stationary symbol sequences, retaining the fluctuation information of the original data.

However, PSTE ignores that the main difference between industrial processes and the financial market lies in the disparate inner mechanism behind nonstationary characteristics, i.e., time delay information. For industrial processes, the nonstationary

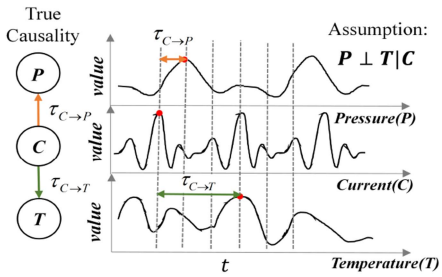

Fig. 1. Illustration of different time delays of nonstationary causality between variables under different control loops. Here, the three variables exemplified are pressure(*P*), current (*C*), and temperature (*T*). The ground truth causalities are $C \to P$ and $C \to T$ with the assumption that $P \perp T|C$.

characteristic is often accompanied by the time delay between variables, revealing the effects of different control loops [26]. Therefore, a causal tool with time delay estimation function and nonstationary adaptability has become an urgent industrial application requirement.

III. Methodology

A. Problem Statement and Motivation

Influenced by various operation conditions that change frequently, industrial processes show typical nonstationary characteristics [1]. Moreover, operation conditions are dominated by different physicochemical phenomena. Thus, time delays are common between different variables. As a result, nonstationary characteristics and time delay usually coexist in industrial processes [26], [27] and should be considered thoroughly. Based on the above analysis, the motivations of this article can be concluded as follows:

1) For the complex nonstationary industrial process, a novel root cause diagnosis strategy is an urgent need to solve the dilemma that traditional methods cannot adapt to nonstationary processes;
2) For multivariate interacting systems of industry, the proposed model must consider how to exclude indirect influence from other variables and capture the time delay information between variables;
3) The corresponding causal criterion and causal diagram construction procedure should be carefully designed to match the proposed root cause diagnosis strategy and boost maintenance efficiency.

Different time delays exist between the causality of variables due to the different mechanisms of control loops. For example, in Fig. 1, assuming that the pressure and temperature variables are completely independent in the case of a known current variable noted as $P \perp T|C$, the current change causes the pressure change through the motor control with a shorter causal time delay $\tau_{C \to P}$, whereas the current increase causes a temperature change through heat conduction with a longer causal time delay $\tau_{C \to T}$. Thus, the causal time delay reflects the control mechanism between process variables.

For causal inference and time delay detection in wide-range nonstationary processes, the following three difficulties should be recognized.

1) Different time delays in causal relationships means information flows in different time scales, as shown in Fig. 1. So, analyzing information transfer in multitimescale is the key to time delay detection.
2) On this basis, the causal inference model needs to be stable under the nonstationary change trends and the indirect effects of intermediate variables within the system.
3) Besides, the matching causal criterion should be carefully designed to avoid confusing bidirectional causality and highlight the significance levels of causal relationships.

B. Multiscale Partial Symbolic Transfer Entropy (MPSTE)

In this part, an MPSTE method is proposed. For nonstationary processes, MPSTE inherits the advantage of segmental symbolization via rank vectors. Especially, the time delay detection goal of MPSTE is achieved via multiscale analysis.

1) Multiscale Filter Module for MPSTE: The multivariate multiscale filter module is designed to distinguish system dynamics on different time scales by filtering. The idea is inspired by Runge *et al.* [20] and Zhao *et al.* [24]. Before the multiscale filter operation, two indispensable assumptions must be clarified.

1) All observed variables in the system are sampled at the same frequency.
2) The sampling interval of the data is shorter than all the true causal time delays [20].

These assumptions ensure that the original data are sufficient to reveal the true causal relationships between variables. Besides, the assumptions can generally be met in real industrial processes.

For an integer subsampling scale τ, the original time series with N samples as $X = [x_1, x_2, \ldots, x_N]$ and $Y = [y_1, y_2, \ldots, y_N]$ can be coarse-grained as

$$\widehat{x}_t^{\,\tau} = \frac{1}{\tau} \sum_{i=(t-1)\tau+1}^{t\tau} x_i, \widehat{y}_t^{\,\tau} = \frac{1}{\tau} \sum_{i=(t-1)\tau+1}^{t\tau} y_i \tag{2}$$

where $\widehat{x}_t^{\,\tau}$ and $\widehat{y}_t^{\,\tau}$ represent the coarse-grained samples of variables X and Y while $t \in [1, N/\tau]$. However, with the increase of scale τ, the amount of data decreases sharply [24].

To solve the issue above, the overlapping multiscale filter module is improved by sliding sample window overlappingly, the formula is written as

$$\widehat{x}_t^{\,\tau} = \frac{1}{\tau} \sum_{i=t}^{t+\tau-1} x_i, \widehat{y}_t^{\,\tau} = \frac{1}{\tau} \sum_{i=t}^{t+\tau-1} y_i \tag{3}$$

where $t \in [1, N - \tau + 1]$. The length of the coarse-grained time series increases from N/τ to $N - \tau + 1$.

Fig. 2 compares the information integration methods with different multiscale filter tricks. The nonoverlapping method shown in Fig. 2(b) is limited by information loss while the overlapping method without delay like Fig. 2(c) introduces strong autocorrelation that obscures the truth of information transfer between variables. So, the overlapping filter method with a certain time delay τ as Fig. 2(d) is the most suitable for the multiscale time delay detection of MPSTE.

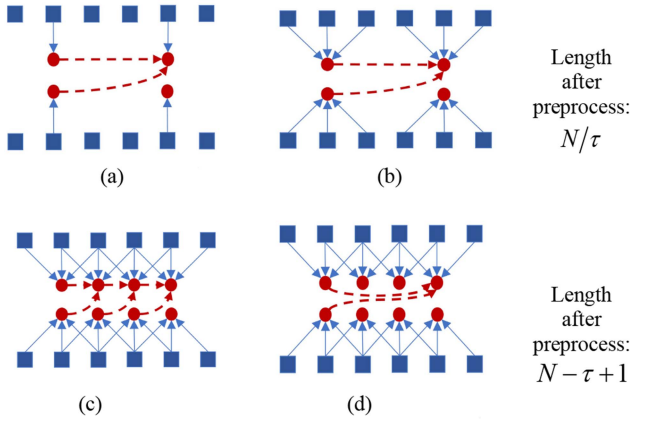

Fig. 2. Schematic diagram for different filters. Here, consider one-step information transitions between two time series with $k = l = 1$ and $\tau = 3$. (a) Original data with random filter of MPSTE. (b) Nonoverlapping multiscale filter of MPSTE. (c) Overlapping multiscale filter of MPSTE without delay. (d) Overlapping multiscale filter of MPSTE with delay.

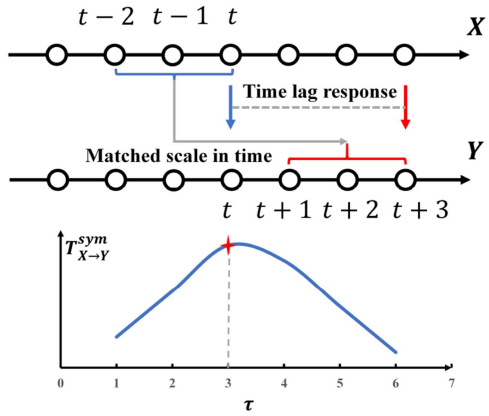

Fig. 3. Schematic of the MPSTE. The scale corresponding to the maximum of $T^{\text{sym}}_{X\to Y}$ is the true time delay between X and Y.

2) Modeling Procedure of MPSTE: For a nonstationary multivariate process, the modeling procedure of MPSTE is summarized as follows:

Step 1. Time-series data multiscale down-sampling and embedding: Filter all the original time series at scale τ using (3) and yield the variables set $\{\widehat{X}^{\tau}, \widehat{Y}^{\tau}, \widehat{Z}_1{}^{\tau} \ldots, \widehat{Z}^{\tau}{}_{M-2}\}$ with the length of each variable is $N' = N - \tau + 1$, and the number of variables is M. Reconstruct each variable $\widehat{X}^{\tau}$ as an embedding vector matrix $\widehat{X}^{\tau}{}_{\text{delay}}(N_{\text{sw}} \times l_{\text{sw}})$ by slide window method where the window length is l_{sw}, the step size is s, and $N_{\text{sw}} = N' - (l_{\text{sw}} - 1) \times s$. Each row of the matrix represents an embedding vector.

Step 2. Nonstationary series transformation and MPSTE estimation: Like PSTE, the embedding vector can be transformed into a rank vector $\widetilde{\mathbf{x}}^{\tau}_{\mathbf{t}} = [r^{\text{sym}}_1, \ldots, r^{\text{sym}}_{l_{\text{sw}}}]$, where $r^{\text{sym}}_* \in r^{\text{sym}}$, $\mathrm{r}^{\text{sym}} = \{0, 1, \ldots, (l_{\text{sw}} - 1)\}$. There are $l_{\text{sw}}!$ kinds of possible permutations for the rank vectors, where $l_{\text{sw}}! = l_{\text{sw}} \times (l_{\text{sw}} - 1) \times \ldots \times 1$ denotes the factorial of l_{sw}. After iterating over N_{sw} embedding vectors, the embedding vector matrix can be transformed into the rank matrix $\widetilde{\mathbf{X}}^{\tau}(N_{\text{sw}} \times l_{\text{sw}})$.

For two variables X and Y, the other variables in the system are defined as environment variables $Z = \{Z_1, \ldots, Z_{M-2}\}$. The most crucial step is to calculate MPSTE (τ) from X to Y under the condition of Z denoted as $T^{\text{sym}}_{X\to Y|Z}(\tau)$ at a certain scale

$$T^{\text{sym}}_{X\to Y|Z}(\tau) = \sum p(\widetilde{\mathbf{y}}^{\tau}_{\mathbf{t}+\tau}, \widetilde{\mathbf{y}}^{\tau}_{\mathbf{t}}, \widetilde{\mathbf{x}}^{\tau}_{\mathbf{t}}, \widetilde{\mathbf{z}}^{\tau}_{\mathbf{t}}) \times \log \frac{p(\widetilde{\mathbf{y}}^{\tau}_{\mathbf{t}+\tau} | \widetilde{\mathbf{y}}^{\tau}_{\mathbf{t}}, \widetilde{\mathbf{x}}^{\tau}_{\mathbf{t}}, \widetilde{\mathbf{z}}^{\tau}_{\mathbf{t}})}{p(\widetilde{\mathbf{y}}^{\tau}_{\mathbf{t}+\tau} | \widetilde{\mathbf{y}}^{\tau}_{\mathbf{t}}, \widetilde{\mathbf{z}}^{\tau}_{\mathbf{t}})} \tag{4}$$

The marginal probability distribution of a variable is equivalent to the frequency of each kind of rank vectors in the symbol matrix corresponding to the variable. The formula is written as

$$p(\tilde{\mathbf{x}}^{\tau}_{\mathbf{t}}) = \frac{n_{\tilde{x}^{\tau}_t}}{N_{\text{sw}}} \tag{5}$$

where $\tilde{x}^{\tau}_t \in S_{l_{\text{sw}}}$, and $n_{\tilde{x}^{\tau}_t}$ is the number of occurrences of the permutation $\tilde{x}^{\tau}_t$ during the observation period.

By the same token, it follows that the joint probability can be calculated by

$$p\left(\widetilde{\mathbf{y}}^{\tau}_{\mathbf{t}+\tau}, \widetilde{\mathbf{y}}^{\tau}_{\mathbf{t}}, \widetilde{\mathbf{x}}^{\tau}_{\mathbf{t}}, \widetilde{\mathbf{z}}^{\tau}_{\mathbf{t}}\right) = \frac{n_{\widetilde{\mathbf{y}}^{\tau}_{\mathbf{t}+\tau}, \widetilde{\mathbf{y}}^{\tau}_{\mathbf{t}}, \widetilde{\mathbf{x}}^{\tau}_{\mathbf{t}}, \widetilde{\mathbf{z}}^{\tau}_{\mathbf{t}}}}{N_{\text{sw}}} \tag{6}$$

where $(\widetilde{\mathbf{y}}^{\tau}_{\mathbf{t}+\tau}, \widetilde{\mathbf{y}}^{\tau}_{\mathbf{t}}, \widetilde{\mathbf{x}}^{\tau}_{\mathbf{t}}, \widetilde{\mathbf{z}}^{\tau}_{\mathbf{t}})$ is the concatenation of the corresponding rank vectors, and $n_{\widetilde{\mathbf{y}}^{\tau}_{\mathbf{t}+\tau}, \widetilde{\mathbf{y}}^{\tau}_{\mathbf{t}}, \widetilde{\mathbf{x}}^{\tau}_{\mathbf{t}}, \widetilde{\mathbf{z}}^{\tau}_{\mathbf{t}}}$ is the times that $(\widetilde{\mathbf{y}}^{\tau}_{\mathbf{t}+\tau}, \widetilde{\mathbf{y}}^{\tau}_{\mathbf{t}}, \widetilde{\mathbf{x}}^{\tau}_{\mathbf{t}}, \widetilde{\mathbf{z}}^{\tau}_{\mathbf{t}})$ appears during the sampling period.

Based on (5) and (6), the transition probability can be derived from the Bayesian formula as

$$p\left(\widetilde{\mathbf{y}}^{\tau}_{\mathbf{t}+\tau} \middle| \widetilde{\mathbf{y}}^{\tau}_{\mathbf{t}}, \widetilde{\mathbf{x}}^{\tau}_{\mathbf{t}}, \widetilde{\mathbf{z}}^{\tau}_{\mathbf{t}}\right) = \frac{p\left(\widetilde{\mathbf{y}}^{\tau}_{\mathbf{t}+\tau}, \widetilde{\mathbf{y}}^{\tau}_{\mathbf{t}}, \widetilde{\mathbf{x}}^{\tau}_{\mathbf{t}}, \widetilde{\mathbf{z}}^{\tau}_{\mathbf{t}}\right)}{p(\widetilde{\mathbf{y}}^{\tau}_{\mathbf{t}}, \widetilde{\mathbf{x}}^{\tau}_{\mathbf{t}}, \widetilde{\mathbf{z}}^{\tau}_{\mathbf{t}})} \tag{7}$$

According to the above results, the MPSTE value of scale τ can be obtained by (4).

By considering environment variables Z as the conditional variables, MPSTE can exclude indirect effects of surrounding environmental variables and identify direct causal relationships.

Step 3. Loop the above two steps to get MPSTE in different scales: Calculate $T^{\text{sym}}_{X\to Y|Z}(\tau)$ from $\tau = 1$ to $\tau_{\max}$, and MPSTE is denoted by $\mathrm{MT}^{\text{sym}}_{\mathbf{X}\to\mathbf{Y}|\mathbf{Z}} = [T^{\text{sym}}_{X\to Y|Z}(1), T^{\text{sym}}_{X\to Y|Z}(2), \ldots T^{\text{sym}}_{X\to Y|Z}(\tau_{\max})]$. Generally, $\tau_{\max} \leq 20$.

The multiscale ensemble of MPSTE expands a novel perspective to estimate dynamic information transfer in nonstationary processes. For time delay detection, Faes *et al.* [28] found that there is a peak of TE shown at the time scale corresponding to the true delay of the causal interactions. The same rule goes for MPSTE. Fig. 3 illustrates that only if the time scale of MPSTE matches the true time delay of the causal relationship between X and Y, the transferred information $T^{\text{sym}}_{X\to Y}(\tau)$ reaches the peak of the curve. For other scales, $T^{\text{sym}}_{X\to Y}(\tau)$ decreases

because some spurious cause-effect relationships in time between X and Y were introduced, leading to a distraction of the transferred information, e.g., in Fig. 3, the true information flow is from X_t to Y_{t+3}, when $\tau = 1$, the information that flows from X_t to Y_{t+1} is calculated, then $T^{\text{sym}}_{X\to Y}(1) < T^{\text{sym}}_{X\to Y}(3)$. Therefore, by comparing MPSTE values on multiple scales, the true causal time delay between variables can be determined as the scale corresponding to the maximum MPSTE.

3) Causality Judgment Based on MPSTE: To go further, two causal criteria for MPSTE are designed to identify the causal direction and quantify the significant level of causality. Theoretically, for scale τ, the causal effect is from X to Y if more information flows from X to Y. So, the direct criterion MPSTE-D at scale τ is designed as

$$D^{\tau}_{X\to Y|Z} = T^{\text{sym}}_{X\to Y|Z}(\tau) - T^{\text{sym}}_{Y\to X|Z}(\tau) \tag{8}$$

where $D^{\tau}_{X\to Y|Z} > 0$ denotes X causes Yunder the condition of Z at scale τ while the negative value means the opposite case. This criterion is simple and intuitive. However, when $T^{\text{sym}}_{X\to Y|Z}(\tau)$ and $T^{\text{sym}}_{Y\to X|Z}(\tau)$are small and close to each other, MPSTE-D cannot identify whether there exists a causal relationship between variables by the sign of $D^{\tau}_{X\to Y|Z}$.

To fix the above defect, a significance test for MPSTE (MPSTE-S) is developed. The statistical significance of the MPSTE is assessed by a randomization test with time-shifted surrogates [29].

The null hypothesis H_0: there is no siginificant causal relationship from X to Y under the condition of Z at scale τ.

To test H_0, the distribution of MPSTE (τ) is constructed by adding the original $T^{\text{sym}}_{X\to Y|Z}(\tau)$ to Γ surrogate MPSTE (τ) values calculated by the surrogate series, where Γ is denoted as the number of surrogate series. Then, sort the $\Gamma + 1$ MPSTE values in ascending order. If $T^{\text{sym}}_{X\to Y|Z}(\tau)$ ranks at the tail of the distribution of MPSTE(τ), H_0 is rejected. According to Yu and Huang [30], for the one-side significance test, the p-value can be derived as

$$p\text{-value} = 1 - \frac{r_o - 0.326}{\Gamma + 1 + 0.348} \tag{9}$$

where r_o is the rank of $T^{\text{sym}}_{X\to Y|Z}(\tau)$ in the ordered list of $\Gamma + 1$ values. $p-$value represents the probability of accepting the original hypothesis H_0. The smaller the p-value, the more significant the causal relationship. There exists significant causality from X to Y at scale τ when $p-\text{value} < 0.10$.

In conclusion, MPSTE-D is a reliable criterion for the dataset with strong causality and sufficient data. It is easy to calculate for an intuitional result but insensitive for spurious causality. Compared with MPSTE-D, MPSTE-S is suitable for deciding the presence of weak coupling and excluding spurious causality. The two criteria play an important role in the following causal diagram construction part. They are complementary for inferring complex nonstationary causality.

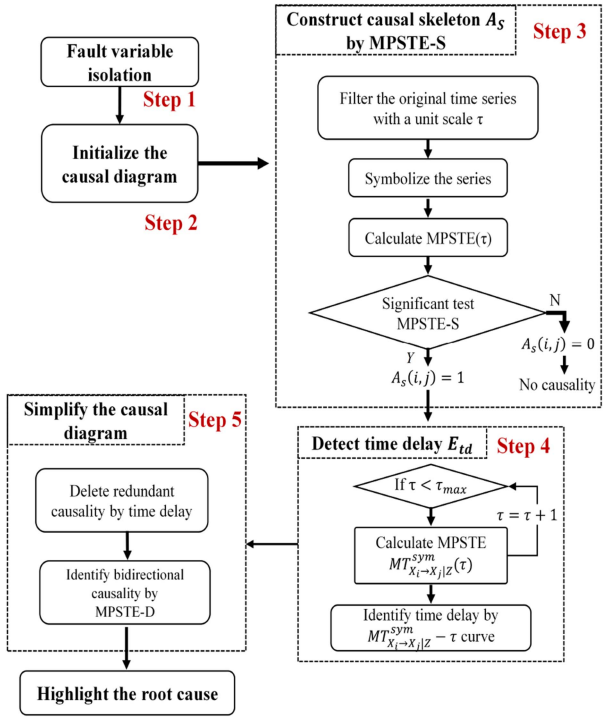

Fig. 4. Flowchart of the proposed strategy to construct causal diagram with time delay.

C. Strategy to Construct the Causal Diagram With Time Delay

In this section, a novel strategy is proposed to construct the causal diagram with time delay information for typical faults. Fig. 4 shows the flowchart of the proposed strategy. The detailed procedure is described as follows.

Step 1 (Fault Variables Isolation): Choose the candidate variables responsible for the fault using proper fault isolation models [31], [32] according to the requirements of practical application. M_f variables with the largest contributions to the fault are isolated as fault variables set V that indicate possible cause of fault, where M_f denotes the number of the isolated fault variables.

Step 2 (Initialize the Causal Diagram): The causal diagram is a directed acyclic graph, which reflects the causal interactions and time delays of variables when a fault happens. The mathematical form of causal diagram is defined as

$$G_c = (V, A_s, E_{\text{td}}) \tag{10}$$

Where V is the set of nodes in the graph corresponding to the fault variables set obtained by Step 1. $A_s(M_f \times M_f)$ is an adjacent matrix, reflecting whether there exist significant causal relationships between fault variables. A_s constructs the original causal skeleton of fault variables. $E_{\text{td}}(M_f \times M_f)$ is a square matrix, recording the time delays and their corresponding MPSTE values of the existing edges in A_s. Each element e_{td}in E_{td} is an array denoted as $(\tau_{\text{td}}, T^{\text{sym}}_{X_i\to X_j|Z}(\tau_{\text{td}}))$ where $X_i, X_j, Z \in V$, the first term denotes the time delay between the two variables

and the second one is the value of MPSTE from X_i to X_j corresponding to the time delay.

Step 3 (Construct the Causal Skeleton A_s): Select two variables of V as the test variables, while the other variables are conditional variables. From a system-wide perspective, a fault causal skeleton requires a unified time scale τ. Practically, the unified scale is generally set as the sampling interval of the system. Then calculate the two MPSTE(τ) to estimate the bidirectional information flows, following the procedure in Section III-B. According to the results, MPSTE-S is carried out to make full use of fault data and identify the significant level of causality via hypothesis testing. When $p-\text{value} < 0.10$, $A_s(i,j) = 1$, revealing that there exists significant causality from the i th variable to the jth one at scale τ. For the noncausal case, $A_s(i,j)$ is set as 0. The same goes for $A_s(j,i)$. Traverse the nodes set V, and obtain the causal skeleton of the fault A_s.

Step 4 (Detect Time Delays): Each nonzero element in A_s represents a causal edge between the fault variables. For these edges, set a $\tau_{\max}$ and calculate the series of $\mathbf{MT}^{\mathbf{sym}}_{\mathbf{X_i}\to\mathbf{X_j}|\mathbf{Z}}$. The time delay τ_{td} is the time scale that matches the maximum of $\mathbf{MT}^{\mathbf{sym}}_{\mathbf{X_i}\to\mathbf{X_j}|\mathbf{Z}}$. So, the time delay can be detected by drawing the curve of $\mathbf{MT}^{\mathbf{sym}}_{\mathbf{X_i}\to\mathbf{X_j}|\mathbf{Z}}$ and $\mathbf{MT}^{\mathbf{sym}}_{\mathbf{X_j}\to\mathbf{X_i}|\mathbf{Z}}$ changing with τ. Then, the array of causal edge is obtained as $(\tau_{\text{td}}, T^{\text{sym}}_{X_i\to X_j|Z}(\tau_{\text{td}}))$. Similarly, calculate the other edges and obtain E_{td}. So far, the primary causal diagram G_c is established.

Step 5 (Simplify the Causal Diagram and Locate the Root Cause): First, the confusing bidirectional causality remained in G_c can be simplified by the direct criterion MPSTE-D. For a bidirectional causality $X_i \leftrightarrow X_j$ in the original G_C, if the curve of $\mathbf{MT}^{\mathbf{sym}}_{\mathbf{X_i}\to\mathbf{X_j}|\mathbf{Z}}$ lies totally above that of $\mathbf{MT}^{\mathbf{sym}}_{\mathbf{X_j}\to\mathbf{X_i}|\mathbf{Z}}$, causality only exists from X_i to X_j from the perspective of multiscale. Otherwise, the information flows in different directions at different scales. Second, uncertain indirect causality can be excluded by getting rid of the environment variables and comparing the time delays of different causal propagation paths. The detailed description is shown in Section III-D.

Note that the root cause of the fault is the variable that shows abnormality first and affects other variables through the control loop. Thus, in a refined causal diagram, the root cause is the main cause of other fault variables but not the effect of any other variables. Also, the fault propagation path is the causal path from the root cause to the affected fault variables.

The output is a refined causal diagram with time delay, revealing the fault mechanism. For faults in nonstationary industrial processes, the proposed causal diagram construction strategy can clarify the causality with time delay information and highlight the root cause and fault propagation path. The core of this strategy is MPSTE and its criteria, detecting causality and time delays in the nonstationary situation.

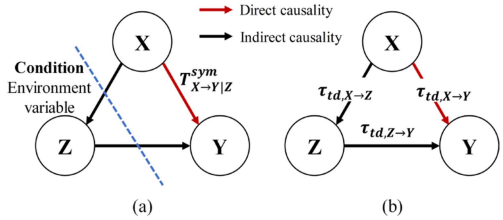

Fig. 5. Schematic of the two mechanisms for MPSTE to identify the indirect causality (a) from the condition variables aspect and (b) from the time delays comparison.

D. Discussion and Discrimination of the Indirect Causality in Multivariate Causal Analysis

In this part, the indirect influence in the multivariate causal analysis is discussed. Also, how can MPSTE identify the direct causality while excluding indirect causality is explained to adapt the complex multivariate industrial system.

For convenience, some studies like TE [15] and MTE [24] usually assume that the variables are not influenced by other variables and only consider the information transfer between two variables. However, in real industrial systems, variables are often coupled and interact with each other and are influenced by other environmental variables in the control loop. The indirect influence of environmental variables may strengthen or weaken the estimation of the causal relationship between two variables [31]. Therefore, to obtain a pure direct causal effect between two variables, it is necessary to discard the influence of the environment. To achieve this, MPSTE estimates the transfer information $T^{\text{sym}}_{X\to Y|Z}$ between a pair of variables X and Y, conditional on the knowledge about the environment variables set Z as in Fig. 5(a). If $T^{\text{sym}}_{X\to Y|Z}$ is near to 0, there exists indirect influence from Z to Y.

Besides, the time delays calculated by MPSTE can also help to simplify the indirect influence. If the direct path delay is less than the sum of indirect path delays, e.g., $\tau_{\text{td},X\to Y} < \tau_{\text{td},X\to Z} + \tau_{\text{td},Z\to Y}$, in Fig. 5(b), then the causality is propagated in the direct path. If indirect causality still exists after these two judgments, more precise methods can be considered, refer to [33].

IV. Verification Study and Discussions

In this section, the proposed causal diagram construction strategy was applied for diagnosing the root cause and analyzing the fault propagation path in the coal mill rig. Real experimental data in normal and faulty operation are used to validate the applicabilities of the proposed methods.

A. Description of Coal Mill Experimental Rig and Coal Blockage Fault

As a prelude for the practical application, this section provides a brief introduction to the coal mill experimental platform, analyzes the nonstationary characteristic of the coal mill process, and clarifies the real fault mechanism of significant coal blockage situations.

1) Brief Introduction to Coal Mill Experimental Rig: The schematic of the coal mill experiment rig is shown in Fig. 6 [7].

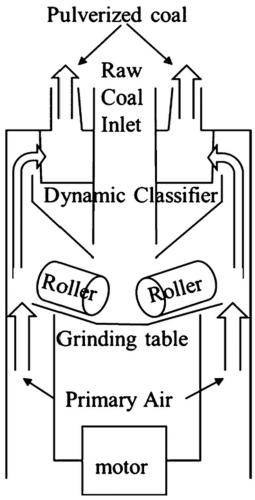

Fig. 6. Working schematic of the coal mill process [10].

TABLE I
DESCRIPTION OF FAULT VARIABLES FOR COAL MILL

No.	Descriptions	Units	Nonstationary (True (T)/ False (F))
T_{en}	Environment temperature	°C	T
T_{mb}	Motor bearing temperature	°C	T
T_{pg}	Planetary gear bearing temperature	°C	T
I_{rs}	Rotary separator motor current	A	F
n_{rs}	Rotary separator rotational speed	r/min	T
T_{out}	Output coal-air mixture temperature	°C	F
T_{in}	Input primary air temperature	°C	T
d_c	Cold air adjusting door opening degree	%	F
ΔP_{mil}	Mill differential pressure between sealed air and cold primary air	Mpa	T
d_h	Hot air adjusting door opening degree	%	F

The conveyor belt in the mill delivers the raw coal to the grinder for crushing. The primary fan dries the pulverized coal and blows it into the rotary separator. The separator feeds fine coal powder into the boiler while coarse coal powder falls back to the grinding table by gravity. Influenced by the harsh operating environment and the croupled control loops, the coal mills operation process shows typical wide-range nonstationary characteristics. Physical mass balance and heat balance relationships exist simultaneously in the coal mill system [34].

2) Experimental Data Preparation: The coal mill experiment rig includes 36 measured process variables. According to the result of ADF test [35], there are 27 nonstationary variables in the coal mill system, reflecting that the process is wide range nonstationary. The nonstationarity of variables depends on the operation mechanism of the system itself and the feedback control loop in which the variables locate. Table I shows the nonstationarity results of some fault variables estimated by the ADF test, where T for the true nonstationary variables and F for the false ones.

We collected 3800 samples with a sampling interval of 1min from the coal mill rig. During the sampling period, coal blockage fault occurred in the coal mill machine.

3) Fault Mechanism of Coal Blockage: Coal blockage can be caused by various reasons, such as a decrease of grinding capacity, low primary airflow, excess coal feed, or high coal powder moisture [34]. In this article, verified by experienced senior professionals, the abnormality in the rotary speed of the rotary separator was the root cause of the coal blockage failure. During the observation period, the abnormal decrease of the rotary separator speed. Thus, the coal powder could not be separated and fell back to the grinding table. The repeated grinding made the grinding efficiency decrease, and finally, the coal blockage failure occurred.

As for the fault propagation process, fault impact started from the variables on the rotary separator, and affected the valve opening degree of the primary air, then the differential pressure inside the coal mill. As time passed, the failure gradually spread through the control loops and more variables were affected. Eventually, an alarm was triggered due to the outlet temperature falling below the standard threshold.

B. Critical Fault Variables Isolation

When a coal blockage fault occurs, many process variables of the coal mill fluctuate abnormally. To capture the main variables affected by the fault and lay a solid foundation for subsequent causal analysis, the first step is using PCA to detect the fault and isolate fault variables, as illustrated in Section III. The detailed calculation process was described in [36]. PCA detected that the fault began at the 2700th min. The remaining 1100 sample points were used for variable fault contribution calculation and causal analysis. In Table I, the top 10 variables with the largest average contributions of 100 fault samples after alarm were isolated as key fault variables to prevent the disturbance from fault evolution.

C. Root Cause Diagnosis and Fault Propagation Path Analysis

After selecting the key fault variables, the proposed strategy to construct the causal diagram with time delay was applied on the coal mill fault data to diagnose the root cause of coal blockage failure. Moreover, conditional variables and time delay information simplified the fault propagation path. The results were analyzed and validated by the fault mechanism.

1) Root Cause Diagnosis Result: According to Step 3 of the proposed strategy, MPSTE-S was used to analyze whether there existed a significant causal relationship between two fault variables. The result of MPSTE-S was displayed in Fig. 7, the number in each square refers to the $p-\text{value}$ of the corresponding variables. The darker the square, the strong the causality is. If $p-\text{value}$ is lower than 0.10, it means that the causal relationship between the tested variables is significant. Thereby the basic causal skeleton A_s was decided as shown in Fig. 10(a).

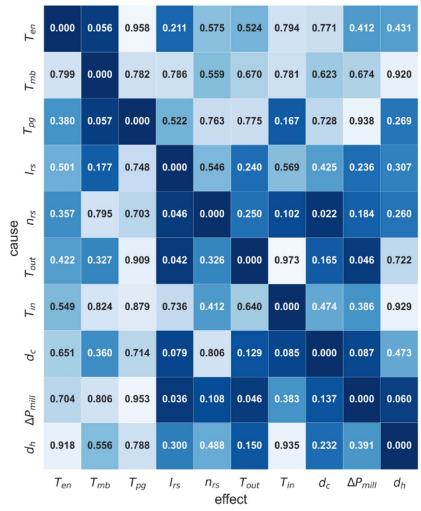

Fig. 7. Significant level of the causality generated by MPSTE-S. The more significant, the bluer.

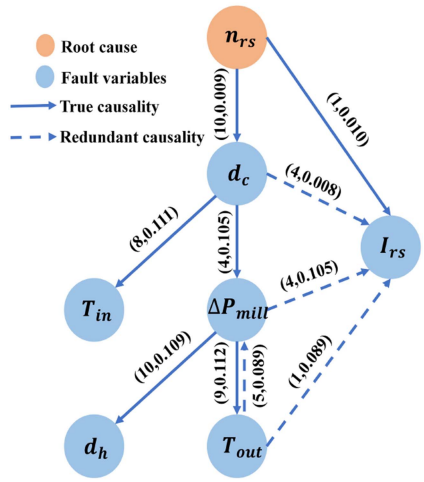

Fig. 8. Causal diagram with time delay of coal mill blockage failure generated by MPSTE.

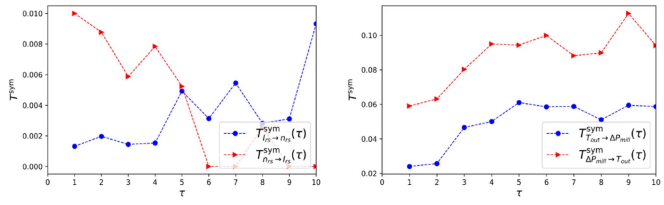

(a) (b)

Fig. 9. MPSTE changes with τ in coal mill system (a) for variables I_{rs} and n_{rs} and (b) for variables ΔP_{mil} and T_{out}.

In Fig. 7, the causal framework was divided into two parts: the part in the lower right from I_{rs} was the main causal transfer skeleton motivated by the coal blockage fault data, showing the root cause of the coal blockage fault and the chief propagation path of the fault; the first three variables in the upper left were isolated from the main causal skeleton because there is no significant causal information transfer between them and the main skeleton. Therefore the root cause should be diagnosed from the main fault causal structure.

According to the main causal structure in Fig. 7, the rotary separator speed n_{rs} is detected as the root cause variable of the coal blockage fault since n_{rs} only affects other variables while it would not be influenced by the others. Thus, this root cause diagnosis result is consistent with expert judgment and mechanistic knowledge [34], which confirms the validity of our proposed strategy.

2) Fault Propagation Path Simplification and Time Delay Validation: The initial fault propagation path can be identified from the main causal skeleton in Fig. 7, which is matching the fault evolution mechanism in Section IV-A. The result showed in Fig. 8 that the abnormal reduction of the rotary separator speed n_{rs} caused the accumulation of coal powder. Thus, the cold air regulating door d_c was closed, resulting in a change in mill differential pressure ΔP_{mil}, and consequently reduced the outlet temperature of the coal mill T_{out}. Moreover, coal blockage led to a reduction in the grinding output of the mill, and the change in n_{rs}, d_c, ΔP_{mil}, and T_{out} is directly reflected in motor current I_{rs}, which is the power evaluation index which seriously affects the coal grinding efficiency.

However, some indirect and spurious causalities still remained in the initial result as the dashed line in Fig. 8. Especially, many fault variables (such as n_{rs}, d_c, and so on) could affect the coal mill output efficiency, producing a complex causal effect on the current I_{rs} , which is confusing for fault propagation tracing. So the skeleton needed to be refined by the time delay information as Steps 4 and 5 in Section III.

Through the comparison of MPSTE on multiple scales, the time delays were calculated and displayed in Fig. 8. For an MPSTE pair in Fig. 9(a) like $(1, 0.010)$, it means that the time delay is 1 min from n_{rs} to I_{rs} and the MPSTE with $\tau = 1$ is 0.010. For bidirectional causality between T_{out} and ΔP_{mil}, causality from T_{out} to ΔP_{mil} can be excluded according to MPSTE-D as shown in Fig. 9(b). Based on the simplification rules for indirect causality in Section III-D, the time delay of the causal relationship from n_{rs} to I_{rs} is the smallest between that of other parents to I_{rs} and it is directly from the root cause, so only this relationship should be remained and other edges to I_{rs} may be indirect links accumulated in the process of fault transmission.

The results in Fig. 8 verify that there exist different time delays in the transmission of causal information between different variables which is related to the control mechanism. In Fig. 8, the abnormality in speed feedback n_{rs} causes the fluctuation of motor current feedback I_{rs} with just 1 min delay. The time delays for differential pressure ΔP_{mil} affecting hot air opening d_h and outlet temperature T_{out} are 10 and 9 min, correspondingly. The result is consistent with the mechanism that the electrical control loop influences other variables rapidly, whereas feedbacks between signals involving temperature and pressure are slower. The time delay information of causality can help the operators understand the development of the fault and improve troubleshooting efficiency.

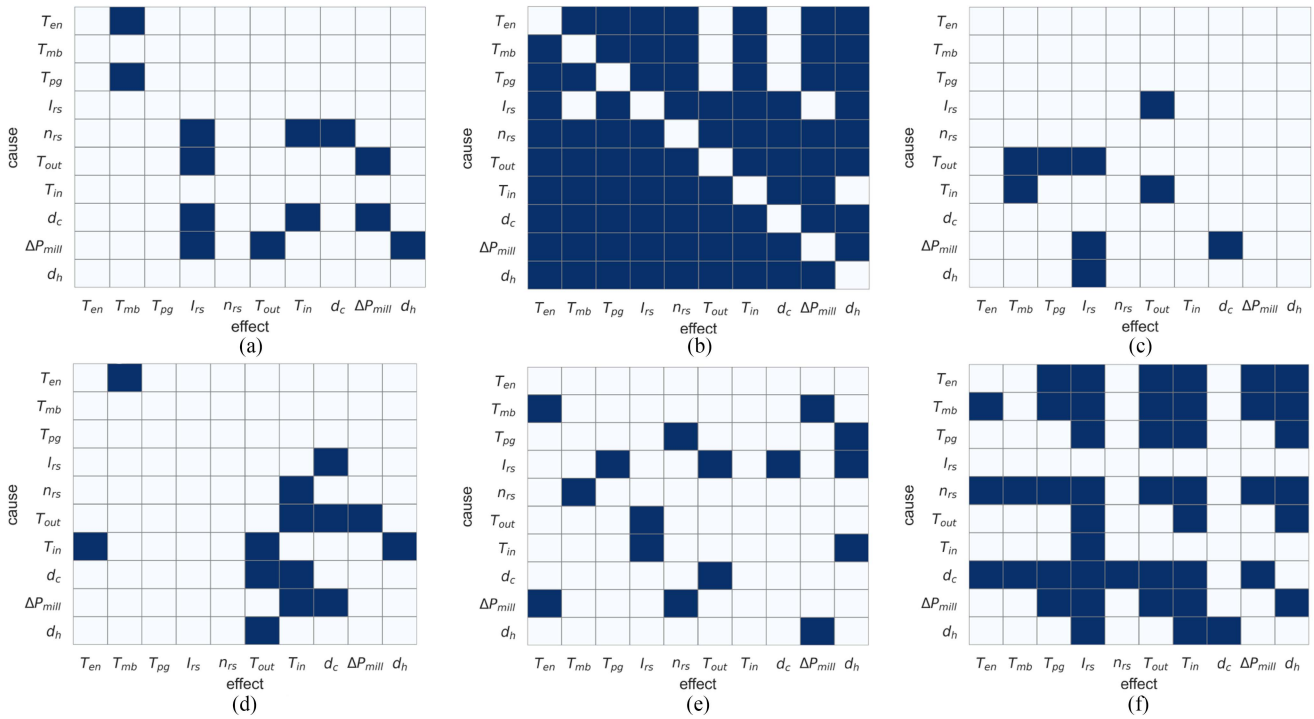

Fig. 10. Comparison results of the coal blockage fault by (a) MPSTE-S, (b) MVGC [8], (c) PTE [9], (d) MSTE-S [37], (e) Lasso Granger [38], and (f) MTE [24]. The causal elements are shown in blue. The proposed (a) MPSTE-S and (d) MSTE-S can identify the true root cause n_{rs} by partial symbols in the nonstationary process of the coal mill rig.

TABLE II
PARAMETER TUNING OF THE CAUSAL METHODS

Causal Method	Parameter Tuning	Significant threshold
MPSTE-S	$h=1$, $t'=1$, $l_{sw}=2$, $\tau=1$	90%
MSTE [37] -S	$h=1$, $t'=1$, $l_{sw}=2$, $\tau=1$	90%
MVGC [8]	$\max lag=5$	90%
Lasso-Granger [38]	$\max lag=5$, $\lambda=0.01$	–
PTE [9]	$h=1$, $t'=1$, $\eta=10$	90%
MTE [24]	$h=1$, $t'=1$, $\eta=10$, $\tau=1$	–

D. Comparisons With the Existing Methods

In this part, the proposed MPSTE-S method was compared with five existing methods including MSTE [37], the commonly used MCGC [8], PTE [9] and their improved versions Lasso Granger [38], and MTE [24]. MSTE is first proposed for classification [37]. Here to adapt it for the causal inference task, it is improved as MSTE-S by the proposed causal criterion and tested in our causal framework. The parameters of the comparison method were set as Table II, where $t'=1$ means that the sampling interval is 1 min, $\max lag$ is the maximum number of points in the past time in the Granger regression models, λ is the sparse penalty coefficient, and η denotes the number of nearest members used to estimate the transfer probability. The performance of the root cause diagnosis task can be valued by whether the true root cause is detected and whether indirect or spurious causalities that cannot fit the fault mechanism are introduced.

Fig. 10 shows the results. It can be seen that only MPSTE-S (proposed) and MSTE-S can identify the true root cause n_{rs}. This proves that the segmental symbolization is useful for handling the causal inference of nonstationary time series. MVGC leads to too many redundant and spurious causalities. It is because that nonstationary trends can cheat the regression model of MVGC into thinking that many variables are causally related. Lasso Granger includes a key variable selection step in the regression process that eliminates many redundant relationships but remains some causalities that do not match the mechanism. PTE leaves out some key causalities while the true root cause is isolated. Compared with methods that ignore the indirect influence (MSTE, MTE), the result of the proposed MPSTE is clearer and closer to the true fault mechanism. To summarize, the MPSTE method is effective for root cause diagnosis in nonstationary multivariate industrial processes.

V. CONCLUSION

In this article, MPSTE was proposed to solve two main challenges in root cause diagnosis. One is detecting direct causality for nonstationary multivariate industrial processes. The other is analyzing the time delay of causality to explain the inner mechanism and simplify the indirect relationships. For the first one, MPSTE used segmental symbolization to transform the nonstationary time series and estimated information transfer while considering multivariate indirect effects. For the second one, the multivariate multiscale filter module of MPSTE was

designed for time delay detection by analyzing information transfer in different scales. Then, a strategy was designed to generate a causal diagram with time delay by MPSTE and verified by a real coal mill experiment rig. The result showed that the time delay of the causal diagram could help simplify the fault propagation path and highlight the root cause, reflecting the fault mechanism of the coal mill. Besides, compared with the five existing methods, MPSTE-S performed better as it could diagnose the true root cause of the coal blockage fault and the causal skeleton constructed by MPSTE-S was clear and explainable.

REFERENCES

[1] C. Zhao, J. Chen, and H. Jing, "Condition-driven data analytics and monitoring for wide-range nonstationary and transient continuous processes," *IEEE Trans. Autom. Sci. Eng.*, vol. 18, no. 4, pp. 1563–1574, Oct. 2021.

[2] P. Zhou, R. Zhang, J. Xie, H. Wang, and T. Chai, "Data-driven monitoring and diagnosing of abnormal furnace conditions in blast furnace ironmaking: An integrated PCA-ICA method," *IEEE Trans. Ind. Electron.*, vol. 68, no. 1, pp. 622–631, Jan. 2021.

[3] S. Zhang and C. Zhao, "Slow feature analysis based batch process monitoring with comprehensive interpretation of operation condition deviation and dynamic anomaly," *IEEE Trans. Ind. Electron.*, vol. 66, no. 5, pp. 3773–3783, May 2019.

[4] A. Stief, J. R. Ottewill, J. Baranowski, and M. Orkisz, "A PCA and two-stage Bayesian sensor fusion approach for diagnosing electrical and mechanical faults in induction motors," *IEEE Trans. Ind. Electron.*, vol. 66, no. 12, pp. 9510–9520, Dec. 2019.

[5] Y. Li, W. Cao, W. Hu, Y. Xiong, and M. Wu, "Incipient fault detection for geological drilling processes using multivariate generalized Gaussian distributions and Kullback–Leibler divergence," *Control Eng. Pract.*, vol. 117, 2021, Art. no. 104937.

[6] K. Zhang, B. Jiang, and F. Chen, "Multiple-Model-Based diagnosis of multiple faults with high-speed train applications using second-level adaptation," *IEEE Trans. Ind. Electron.*, vol. 68, no. 7, pp. 6257–6266, Jul. 2021.

[7] Q. Shi and H. Zhang, "Fault diagnosis of an autonomous vehicle with an improved SVM algorithm subject to unbalanced datasets," *IEEE Trans. Ind. Electron.*, vol. 68, no. 7, pp. 6248–6256, Jul. 2021.

[8] H. Chen, Z. Yan, Y. Yao, T. B. Huang, and Y. S. Wong, "Systematic procedure for Granger-causality-based root cause diagnosis of chemical process faults," *Ind. Eng. Chem. Res.*, vol. 57, no. 29, pp. 9500–9512, 2018.

[9] M. Bauer, J. W. Cox, M. H. Caveness, and J. J. Downs, "Finding the direction of disturbance propagation in a chemical process using transfer entropy," *IEEE Trans. Control Syst. Technol.*, vol. 15, no. 1, pp. 12–21, Jan. 2007.

[10] C. Tian and C. Zhao, "Single model-based analysis of relative causal changes for root-cause diagnosis in complex industrial processes," *Ind. Eng. Chem. Res.*, vol. 60, no. 34, pp. 12602–12613, 2021.

[11] Z. Chai, C. Zhao, and B. Huang, "Multisource-Refined transfer network for industrial fault diagnosis under domain and category inconsistencies," *IEEE Trans. Cybern.*, May 2021, doi: 10.1109/TCYB.2021.3067786.

[12] R. Engle and C. Granger, "Co-integration and error correction: Representation, estimation, and testing," *Econometrica: J. Econometric Soc.*, vol. 55, pp. 251–276, 1987.

[13] C. Zhao, W. Wang, C. Tian, and Y. Sun, "Fine-scale modelling and monitoring of wide-range nonstationary batch process: From viewpoint of closed-loop control," *IEEE Trans. Ind. Electron.*, vol. 68, no. 9, pp. 8808–8818, Sep. 2021.

[14] L. Barnett, A. B. Barrett, and A. K. Seth, "Granger causality and transfer entropy are equivalent for Gaussian variables," *Phys. Rev. Lett.*, vol. 103, no. 23, 2009, Art. no. 238701.

[15] M. Bauer, J. W. Cox, M. H. Caveness, J. J. Downs, and N. F. Thornhill, "Finding the direction of disturbance propagation in a chemical process using transfer entropy," *IEEE Trans. Control Syst. Technol.*, vol. 15, no. 1, pp. 12–21, Jan. 2007.

[16] W. Yu, C. Zhao, and B. Huang, "Recursive cointegration analytics for adaptive monitoring of nonstationary industrial processes with both static and dynamic variations," *J. Process Control*, vol. 92, pp. 319–332, 2020.

[17] M. Staniek and K. Lehnertz, "Symbolic transfer entropy," *Phys. Rev. Lett.*, vol. 100, no. 15, 2008, Art. no. 158101.

[18] A. Papana, C. Kyrtsou, D. Kugiumtzis, and C. Diks, "Detecting causality in nonstationary time series using partial symbolic transfer entropy: Evidence in financial data," *Comput. Econ.*, vol. 47, no. 3, pp. 341–365, 2016.

[19] X.-C. Shangguan *et al.*, "Robust load frequency control for power system considering transmission delay and sampling period," *IEEE Trans. Ind. Inform.*, vol. 17, no. 8, pp. 5292–5303, Aug. 2020.

[20] J. Runge *et al.*, "Inferring causation from time series in earth system sciences," *Nature Commun.*, vol. 10, no. 1, pp. 1–13, 2019.

[21] J. Borge-Holthoefer *et al.*, "The dynamics of information-driven coordination phenomena: A transfer entropy analysis," *Sci. Adv.*, vol. 2, no. 4, 2016, Art. no. e1501158.

[22] Y. Shu and J. Zhao, "Data-driven causal inference based on a modified transfer entropy," *Comput. Chem. Eng.*, vol. 57, pp. 173–180, 2013.

[23] H. Ye, E. R. Deyle, L. J. Gilarranz, and G. Sugihara, "Distinguishing time-delayed causal interactions using convergent cross mapping," *Sci. Rep.*, vol. 5, no. 1, pp. 1–9, 2015.

[24] X. Zhao, Y. Sun, X. Li, and P. Shang, "Multiscale transfer entropy: Measuring information transfer on multiple time scales," *Commun. Nonlinear Sci. Numer. Simul.*, vol. 62, pp. 202–212, 2018.

[25] N. Zhang, A. Lin, and P. Shang, "Multiscale symbolic phase transfer entropy in financial time series classification," *Fluctuation Noise Lett.*, vol. 16, no. 2, 2017, Art. no. 1750019.

[26] C. Zhang, F. Long, Y. He, W. Yao, L. Jiang, and M. Wu, "A relaxed quadratic function negative-determination lemma and its application to time-delay systems," *Automatica*, vol. 113, 2020, Art. no. 108764.

[27] W. Du, M. Kang, and M. Pecht, "Fault diagnosis using adaptive multifractal detrended fluctuation analysis," *IEEE Trans. Ind. Electron.*, vol. 67, no. 3, pp. 2272–2282, Mar. 2020.

[28] L. Faes, N. Giandomenico, and P. Alberto, "Compensated transfer entropy as a tool for reliably estimating information transfer in physiological time series," *Entropy*, vol. 15, no. 1, pp. 198–219, 2013.

[29] A. Papana, C. Kyrtsou, D. Kugiumtzis, and C. Diks, "Assessment of resampling methods for causality testing: A note on the US inflation behavior," *PLoS One*, vol. 12, no. 7, 2017, Art. no. e0180852.

[30] G. Yu and C. Huang, "A distribution free plotting position," *Stochastic Environ. Res. Risk Assessment*, vol. 15, no. 6, pp. 462–476, 2001.

[31] W. Yu and C. Zhao, "Sparse exponential discriminant analysis and its application to fault diagnosis," *IEEE Trans. Ind. Electron.*, vol. 65, no. 7, pp. 5931–5940, Jul. 2018.

[32] L. Feng and C. Zhao, "Fault description based attribute transfer for zero-sample industrial fault diagnosis," *IEEE Trans. Ind. Inform.*, vol. 17, no. 3, pp. 1852–1862, Mar. 2021.

[33] P. Duan, F. Yang, T. Chen, and S. Shah, "Direct causality detection via the transfer entropy approach," *IEEE Trans. Control Syst. Technol.*, vol. 21, no. 6, pp. 2052–2066, Nov. 2013.

[34] Y. Jian, X. Qing, Y. Zhao, L. He, and X. Qi, "Application of model-based deep learning algorithm in fault diagnosis of coal mills," *Math. Problems Eng.*, vol. 2020, pp. 1–14, 2020.

[35] D. A. Dickey and W. A. Fuller, "Distribution of the estimators for autoregressive time series with a unit root," *J. Amer. Stat. Assoc.*, vol. 74, no. 366a, pp. 427–431, 1979.

[36] L. H. Chiang, E. L. Russell, and R. D. Braatz, "Fault diagnosis in chemical processes using Fisher discriminant analysis, discriminant partial least squares, and principal component analysis," *Chemometrics Intell. Lab. Syst.*, vol. 50, no. 2, pp. 243–252, 2000.

[37] W. Yao and J. Wang, "Multi-scale symbolic transfer entropy analysis of EEG," *Physica A: Stat. Mech. Appl.*, vol. 484, pp. 276–281, 2017.

[38] A. Arnold, Y. Liu, and N. Abe, "Temporal causal modeling with graphical granger methods," in *Proc. 13th ACM SIGKDD Int. Conf. Knowl. Discov. Data Mining*, 2007, pp. 65–75.

Shuyu Duan received the B.Eng. degree in systems and control engineering from the College of Electronics and Information, Northwestern Polytechnical University, Xi'an, China, in 2020. She is currently working toward the M.S. degree in control science and engineering with the College of Control Science and Engineering, Zhejiang University, Hangzhou, China.

Her research interests include statistical data analysis, causal analysis, and fault diagnosis.

Chunhui Zhao (Senior Member, IEEE) received the B.Eng., M.S., and Ph.D. degrees in control science and engineering from the Department of Automation, Northeastern University, Shenyang, China, in 2003, 2006, and 2009, respectively.

Since January 2012, she has been a Professor at the College of Control Science and Engineering, Zhejiang University, Hangzhou, China. She has authored or coauthored more than 200 papers in peer-reviewed international journals and conferences. Her research interests include statistical process monitoring, fault diagnosis, and glucose control.

Dr. Zhao was a recipient of the National Top 100 Excellent Doctor Thesis Nomination Award, New Century Excellent Talents in University, China, and National Science Fund for Excellent Young Scholars. She was a Postdoctoral Fellow (from January 2009 to January 2012) at the Hong Kong University of Science and Technology, Hong Kong, and the University of California, Santa Barbara, Los Angeles, CA, USA.

Min Wu (Fellow, IEEE) received the B.S. and M.S. degrees in engineering from Central South University, Changsha, China, in 1983 and 1986, respectively, and the Ph.D. degree in engineering from Tokyo Institute of Technology, Tokyo, Japan, in 1999.

He was a Faculty Member of the School of Information Science and Engineering at Central South University from 1986 to 2014, and was promoted to Professor in 1994. In 2014, he joined China University of Geosciences, Wuhan, China, where he is currently a Professor with the School of Automation. He was a Visiting Scholar with the Department of Electrical Engineering, Tohoku University, Sendai, Japan, from 1989 to 1990, and a Visiting Research Scholar with the Department of Control and Systems Engineering, Tokyo Institute of Technology, from 1996 to 1999. From 2001 to 2002, he was a Visiting Professor at the School of Mechanical, Materials, Manufacturing Engineering and Management, University of Nottingham, Nottingham, U.K. His current research interests include process control, robust control, and intelligent systems.

Dr. Wu is a Fellow of the Chinese Association of Automation. He was the recipient of the IFAC Control Engineering Practice Prize Paper Award in 1999 (together with M. Nakano and J. She).